A comparative study of using geophysical methods for imaging subsurface voids of various sizes and at different depths

M. Rahimi [a], C.M. Wood [a,*], Loukas F. Kallivokas [b]

[a] Department of Civil Engineering, University of Arkansas, Fayetteville, AR 72701, USA
[b] Fariborz Maseeh Department of Civil, Architectural and Environmental Engineering, The University of Texas at Austin, Austin, TX 78712, USA

ARTICLE INFO

ABSTRACT

Subsurface voids pose significant geohazards, underscoring the need for their timely detection in order to mitigate the associated hazard. We report on a field study aimed at the comparative assessment of electrical resistivity tomography (ERT), seismic refraction tomography (SRT), and the multichannel analysis of surface waves (MASW) for void mapping in karstic regions. The field surveys were conducted at a site in central Texas, of typical karstic geomorphology, and involved the co-located deployment of ERT, SRT and MASW arrays. Post-surveying, boreholes were drilled at select locations for verification purposes. It is shown that MASW demonstrated limited ability to resolve voids due to its inherent theoretical limitations. In contrast, ERT revealed high-resistivity air-filled zones, and low-resistivity soil-filled regions, which aligned well with post-survey borehole logs, although deeper voids remained largely undetected. SRT clearly delineated voids through velocity reductions, but smoothing effects overestimated void velocities. Using ERT and SRT jointly provided improved void characterization compared to single-method-based interpretations, with ERT determining void type and SRT delineating boundaries. Despite the relative success of the joint ERT-SRT application, it is evident that without the corroboration provided by invasive testing, definitive void localization and characterization under arbitrary site conditions remains elusive.

1. Introduction

The presence of underground voids and cavities poses significant geohazards and engineering challenges in many regions worldwide. Sinkholes, natural caves, abandoned mines, karstic geology, and underground urban infrastructure can each lead to subsidence, collapses, and catastrophic failures without prior signs of ground instability. Sinkhole collapses originating from the presence of underground voids have caused substantial economic losses and environmental damage throughout history. In 1981, a sinkhole, formed suddenly in Winter Park, Florida, swallowed parts of several residential and commercial buildings, resulting in over $4 million damage. The catastrophic 1994 collapse of the Retsof salt mine near Cuylerville, New York created a giant sinkhole that caused environmental damage, resulting in remediation costs in excess of $12 million. Undetected subsurface voids can be triggered by hydraulic changes, loading events, vibrations, or even minor seismic activity, underscoring the need for early void detection to mitigate hazard during construction (Karaman and Karadayılar, 2004). However, the complex void morphology and the spatially heterogeneous

subsurface conditions pose significant challenges, accentuating the need for efficient noninvasive methods to rapidly identify voids over broad areas.

Texas is one of the states where the sinkhole hazard is significant, resulting in substantial property damages each year (Kuniansky et al., 2016). The Central Texas geologic conditions consist of extensive carbonate and evaporite rocks at, or near, the ground surface, which facilitate the formation of underground voids, or the formation of bedrock-collapse sinkholes, as a result of the erosion of the overlying strata (Hunt et al., 2013; Kim et al., 2019). This is especially true in the Austin area, where the Lower Cretaceous portion of the Glen Rose Formation and the Edwards Aquifer underlies the city (Saribudak, 2011). The porous nature of limestone allows it to be gradually dissolved by slightly acidic groundwater, slowly forming voids and cavities over time. As surface materials travel downward into newly-formed voids, the ground above can subside or collapse suddenly if the overlain void volume is large enough. These effects highlight the potential severity of sinkhole hazards associated with underground voids, which can risk infrastructure damage, groundwater contamination, injuries, and loss of

---

life. The extensive underground cavities in central Texas frequently impact transportation projects adversely, when encountered during construction. Thus, accurate subsurface characterization is critical to infrastructure in this karstic region to avoid threats posed by unidentified voids and caves.

While an apparent surface fracture may clearly indicate the existence of an underground void, such obvious cases are rare. Rather, targeted subsurface testing is required to confirm the potential void existence; however, blind drilling is not an optimal approach given the low probability of drilling into an actual void (Dobecki and Upchurch, 2006). Instead, geophysical methods, including ground penetrating radar (GPR), electrical resistivity tomography (ERT), and seismic methods such as Multichannel analysis of Surface Waves (MASW), and P-wave refraction can provide a guide for testing locations by identifying subsurface anomalies including voids that may contribute to sinkhole development (Sevil et al., 2017; Rahnema et al., 2021; Wang and Lv, 2023). These noninvasive surveys optimize subsequent coring or drilling operations by increasing the likelihood of intersecting the existing voids or fractures. Ultimately, subsurface testing is essential in detecting the existence of voids and cavities capable of underground collapse.

ERT is an efficient method for detecting underground anomalies such as voids and karstic features (Martinez-Pagan et al., 2013; Arjwech et al., 2021; Liu et al., 2023; Diallo et al., 2023). ERT maps spatial variations in electrical resistivity corresponding to changes in moisture content, porosity, and lithology (Reynolds, 2011). It can reveal low-resistivity anomalies associated with water-filled voids, or high-resistivity areas associated with air-filled voids. However, various environmental factors may result in misleading outcomes (Martinez-Moreno et al., 2015); for example, challenges arise in cases of heterogeneous conditions with variable water saturation and fractured bedrock. A limitation of ERT for void detection is that the inverted location and geometry of underground anomalies can vary based on the parameterization used during the inversion process. Using the measured resistivity data, the inversion process generates a subsurface resistivity map while smoothing the interfaces between different resistivity zones, effectively modifying the precise size and shape of voids. The inversion process can also shift the position of detected voids/anomalies away from their true locations (Deiana et al., 2018). Another key difficulty with electrical resistivity methods is that accurately differentiating between high-density intact rock and air-filled voids is challenging, as both cases can exhibit similarly high-resistivity values (Bharti et al., 2016; Argote et al., 2020). This makes it difficult in some cases to conclusively identify voids based on high resistivity alone. Therefore, while ERT may successfully detect voids, caution must be used when interpreting the exact morphology of voids from the inverted resistivity maps.

Seismic refraction tomography (SRT) using P-waves is capable of detecting interfaces between layers with contrasting velocity properties, including subsurface anomalies indicative of voids (Grandjean and Leparoux, 2004; Martinez-Segura et al., 2024). However, low-velocity air-filled regions indicate a lack of consolidated subsurface material, preventing effective wave propagation. Such velocity discontinuities create distinct first arrival travel-time curve anomalies relative to neighboring consolidated zones, thus delineating void boundaries from surrounding competent ground. However, effectiveness depends on sufficient velocity contrasts with the surrounding formations to generate a recordable refraction event from the void interfaces. Resolution can also vary with array geometry and energy sources used. Studies demonstrate successful application of SRT across sinkholes, tunnels, buried channels and other voids (Jabrane et al., 2023).

MASW utilizes seismic surface waves to probe the subsurface. By laterally interpolating multiple 1D shear wave velocity (Vs) measurements gained through roll-along measurements, a pseudo 2D shear wave velocity Vs section can be developed, which may be able to reveal local velocity contrast suggestive of voids. However, the effectiveness of the 2D MASW for detecting subsurface anomalies such as voids remains unclear, with literature presenting varied successful and unsuccessful

outcomes (Nasseri-Moghaddam et al., 2007; Sloan et al., 2015; Xie et al., 2022). As outlined by Arslan et al. (2021) the array length, receiver spacing, source frequency content, configuration specifics, inversion algorithms, and data processing may influence resolution of the subsurface. Considering basic MASW assumptions, the detection, localization, and material determination of a small, shallow anomaly or void appears to contradict the fundamentals of MASW. Thus, detectability may only be possible under particular circumstances of relatively large and shallow anomalies. Inherent limitations arising from fundamental spatial averaging constraints and decreased resolution with depth may hinder resolution of small-scale subsurface features. Additional case studies are needed to assess the factors impacting reliable imaging across different site conditions using consistent processing and assessment procedures.

Currently, there is no individual technology or method proven to be able to detect and localize reliably and consistently subsurface voids across various geological settings. Site-specific factors such as stratigraphy, lithology, target depth and size may preclude the success of a particular technique at other locations (Sloan et al., 2013). For example, ERT may work well at imaging voids in special scenarios but may fail at sites with different electrical properties. This highlights the importance of selecting appropriate techniques tailored to the specific study goals and field conditions. ERT can be improved through multi-physics approaches aiming at reproducing the subsurface distribution of a material property with other methods like seismic surveying that measures the seismic velocity rather than the electrical resistivity. Multiple data sets obtained through a multi-physics approach can provide more confident interpretation of the subsurface anomalies. Used together, ERT and seismic methods can improve resolution and interpretation reliability for void detection.

This paper presents a comprehensive field application of joint ERT, SRT, and MASW for void detection and subsurface characterization in a karstic environment. The study, conducted at a site in Central Texas known for its karst features, is novel in its simultaneous application of these methods to detect voids of various sizes and depths, including those without apparent surface signatures. We compare the results of ERT, SRT, and MASW surveys with data from several boreholes, providing an instructive opportunity to evaluate the accuracy and reliability of these geophysical methods against ground-truth data. This approach allows for a robust assessment of each method's capabilities and limitations in void detection. Additionally, we discuss the application of pseudo 3D ERT inversion, offering insights into its potential for comprehensive subsurface imaging in complex karst settings. By integrating multiple geophysical techniques and validating results with borehole data, this study contributes significantly to our understanding of effective subsurface characterization strategies in challenging karst environments.

2. Site geologic background

The study site is located along Texas State Highway 29 in Georgetown, TX as shown in Fig. 1. Geophysical investigation was conducted after a void was reported to have formed near the study site, raising concerns about ground stability and subsidence risk in the area. The survey area is close to the Balcones Fault Zone (BFZ), a major fault system running through central Texas. BFZ is a primary boundary between two aquifers in Texas, the Trinity and Edwards aquifers. This fault system was created during the Ouachita Orogeny Mountain building event and is characterized by normal faults that have caused significant vertical displacement of rock units (Saribudak, 2016; Saribudak and Hauwert, 2017). The faulting and fracturing of the limestone and dolomite formations have allowed for the development of underground caves and other voids in the Georgetown area (Sharp Jr et al., 2019). The Edwards Limestone, which underlies much of Georgetown, is riddled with solution cavities, cave systems, and porous vuggy zones due to the dissolution of limestone over time (Howard, 1964). Surface water
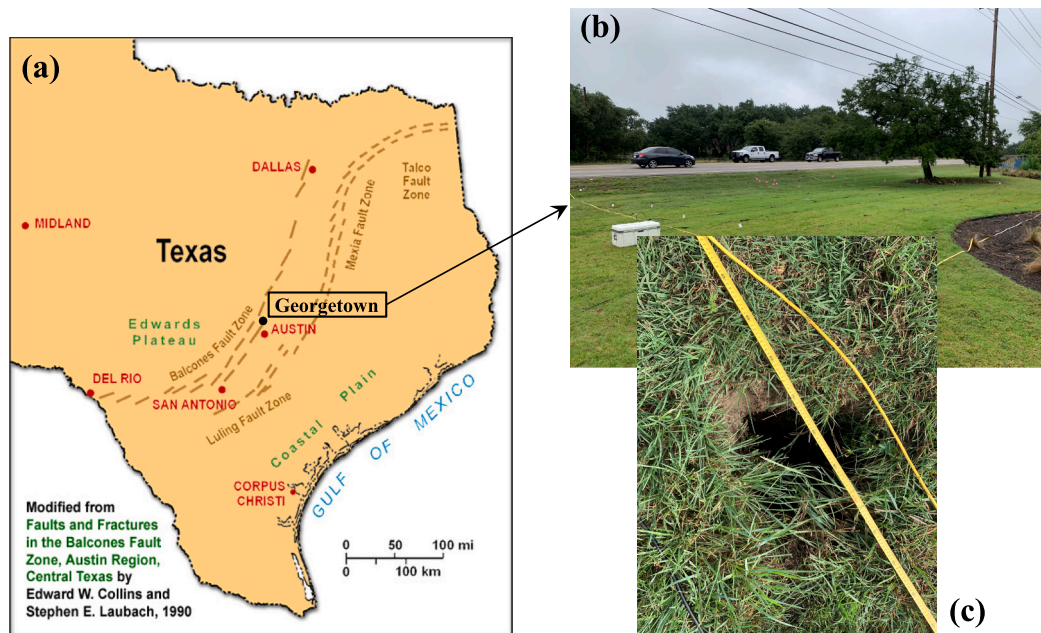
Fig. 1. (a) site location near to BFZ (adopted ftom https://www.beg.utexas.edu/geowonders/centtex), (b) site general view, (c) a void entrance at the ground surface.

penetrates along faults and fractures, gradually dissolving away calcite and dolomite crystals in the rock. This forms extensive underground conduit systems and cave networks within the Edwards Limestone aquifer (Saribudak, 2011).

Further dissolution and collapse along zones of weakness have created sinkholes and other karstic features near the surface. The Mount Bonnell fault at the intersection of Bee Cave Road and Camp Craft Road to the west of Austin downtown is a segment of the Balcones system that has been associated with abundant karstic features (i.e., caves, sinkholes, fractures, and collapsed areas) due to the downward movement of water along faults that dissolves the limestone (Saribudak, 2016). Edwards Limestone on the eastern downthrown side of the faults has experienced more intense karstification (Hunt et al., 2013). The presence of these underground voids and permeability pathways directly impacts groundwater flows and hydrogeology in the Georgetown region. The complex faulting and fracturing of soluble limestone and dolomite formations has allowed for the development of underground caves, sinkholes, enlarged fractures, and other voids that characterize the unique karstic landscape and hydrogeology of the Georgetown area. The geological conditions make the region prone to further sinkhole formation and ground subsidence risks.

3. Geophysical investigations

To investigate the capability of geophysical methods for detecting known voids and characterizing the subsurface, a geophysical study utilizing ERT, jointly with SRT and MASW surveys, was conducted along Texas State Highway 29. The test site is in Georgetown, Texas, at approximately 30.631996°N, −97.761407°W (latitude, longitude), which included a small patch of mostly flat land, sandwiched between Texas State Highway 29 (eastbound) and the Crescent Bluff Subdivision. A site map showing the approximate location of the geophysical survey lines is provided in Fig. 2, showing ERT and seismic survey lines together, as well as borehole locations. The field tests (ERT and MASW)

were conducted on June 29–30, 2021, while in December 2022, a few boreholes were drilled at select locations to verify or refute the presence of suspected voids.[1] It should be noted that the drilling occurred approximately 18 months after the geophysical surveys, and changes (e. g., enlargement or filling of voids) may have occurred in the intervening period. The ground surface was wet during the geophysical testing, with rain in the days prior to the testing date. In the following sections, the testing and data processing parameters are presented in detail for each method.

3.1. Electrical resistivity tomography (ERT)

Nine ERT survey lines were conducted in the study as shown in Fig. 2. The direction of the survey is shown by white arrows. The location of boreholes, a known void, and utility crossing are also shown in Fig. 2. Line X was surveyed first: it runs, approximately, West-East (zero distance on the West end of the line) with a length of 110 m. Lines A-H were surveyed next and run, approximately, West-East with a length of 55 m and parallel to each other, with approximately 2.0 m spacing between lines. However, line G was located 2.2 m from line F and 1.8 m from line H in order to avoid a water line located parallel to the line. The location of four water main valves on the site are shown in Fig. 2. A surface opening (void opening) was located at 36.5 m along line B and 43 m along line X as shown in Fig. 1c and Fig. 2. Overhead electrical service lines and other underground utilities were present at various locations throughout the project site. These tend to interfere with the measured resistivity values, which, in turn, may impact subsurface anomaly/void detectability and characterization. However, these are realistic conditions, which are often encountered during roadside surveys, and should be considered when evaluating the appropriateness of survey methods for a project.

The ERT data were collected using an Advanced Geosciences Inc. (AGI) resistivity meter. For each survey, 56 surface electrodes were used with distances between electrodes of 2 m for Line X and 1 m for Line A-

---

[1] Borings, and subsequent characterization, was performed by Beyond Engineering & Testing, LLC (BEYOND), under Texas Department of Transportation contract 88-1IDP5009.
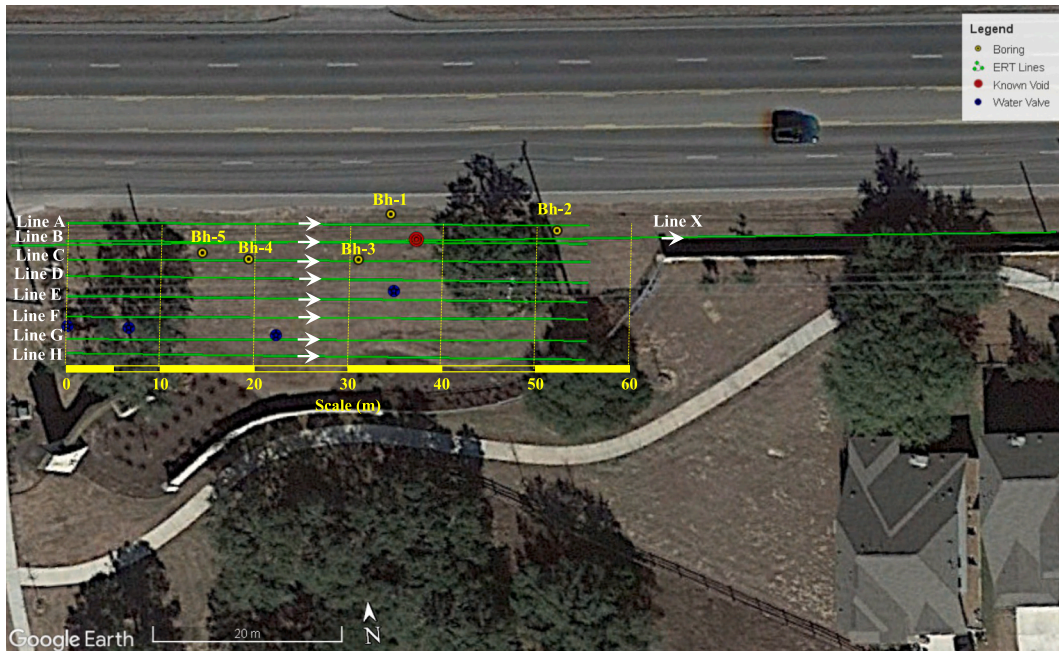
Fig. 2. Site map of ERT testing with lines A-X shown along with borehole locations (Bh-1 through Bh-5), known void entrance, and utility crossing (the white arrows show the direction of the survey).

H. Two-dimensional dipole–dipole and strong gradient survey configurations were used to collect data for each survey. The raw ERT data sets were inverted using AGI's EarthImager2D software. Electrode elevations from the total station were included in the inversions. The misfits between measured and modeled resistivity data for each profile were sought to be minimized during the inversion iterations. The goodness of fit was assessed using the root mean square (RMS) misfit. It is important to note that the RMS misfit represents an average misfit between measured and modeled data across all data points. When comparing RMS misfits from different inversion programs, one must first examine how each inversion software suite defines this metric, as definitions may vary. AGI's software defines RMS by the equation below:

$$RMS(\%) = \sqrt{\frac{\sum_{i=1}^{N} \left(\frac{d_i^{Pred} - d_i^{Meas}}{d_i^{Meas}}\right)^2}{N}} \times 100\%$$

Where N is the total number of measurements, d_{Pred} is the predicted data and d_{Meas} is the measured data. In this study, a final RMS misfit of less than 5–10 % was achieved for each profile after several trials. For the Pseudo 3D processing, the 2D raw resistivity data for Lines A-H were fed in AGI's EarthImager3D software. The resulting 3D resistivity model represents the resistivity distribution that best fits the measured data. It should be mentioned that both 2D and 3D resistivity inversions are characterized by non-uniqueness, that is, there could be several resistivity distributions that match the measured data equally well.

3.2. Pseudo-2D MASW profiling

A total of eight MASW lines (A-H) were surveyed, as shown in Fig. 2, with a length of 47 m approximately in West-East direction (zero distance on the West end of the line, same as ERT lines). The starting points for ERT and seismic survey lines were the same for similar lines, but the MASW lines were shorter. Each MASW line consisted of a linear array of 48, 4.5 Hz vertical geophones with a uniform spacing between geophones of 1 m. Surface waves were generated using a 7.3 kg sledgehammer. The waveforms were recorded using two 24 channel Geometrics Geode seismographs. At each shot location, 5 hits were stacked in order to increase the signal-to-noise ratio.

Subarrays comprising 24 geophones at 1 m spacing, for a total subarray length of 23 m, with each subarray offset by 6 m from the previous array, and 6 shot locations (at 0.5 m, 3.5 m, and 6.5 m off of the two ends of the subarray were used for pseudo-2D profiling. The experimental MASW raw dispersion data with multiple source offsets were combined and processed in MATLAB using the frequency domain beamformer method. Only the fundamental mode was used for the inversion process. The Rayleigh dispersion data were inverted using the Geopsy software package to develop a 1D shear wave velocity (Vs) profile for each subarray. The boring log information was used as a guide to determine the parameterization for the inversion process. The 1D Vs profiles generated for each subarray were then combined to develop a pseudo 2D Vs cross-section for each MASW survey line. It should always be remembered that the spatial averaging effect across the length of the array will tend to smear/distort relatively small features beneath the array, making it difficult to resolve true subsurface variability in the 2D profile.

3.3. Seismic refraction tomography (SRT)

The P-wave refraction survey utilized similar instrumentation and array configurations as implemented in the MASW surveys. P-waves were generated at multiple source locations, 6.5 m off from both ends, and with 3 m spacing along the array. The P-wave seismic refraction data were processed using the Geometrics software package SeisImager, in general accordance with ASTM International, 2018. The number of layers is determined based on the variations in the slope of the lines fit through the P-wave arrival times. Each arrival time included shot location, geophone location along the line, first arrival time, and geophone elevation. First analyses were conducted using the time interval method (TIM) and generalized reciprocal method (GRM). Each seismic arrival time, or "pick," was assigned to an appropriate layer based on the slope of the P-wave arrival times. These picks were then used to determine the refraction paths through the layers. Typically, 3–5 layers could be identified from the arrivals. Following the TIM and GRM modeling, the data were modeled using tomographic analysis. A minimum of 50 iterations of the non-linear raypath inversion were implemented to improve fits to the arrival times. The goodness of the fit

between the experimental (observed) and the inverted model (calculated) was judged based on visual inspection and the magnitude of the root-mean-square (rms) difference.

4. Results and discussion

The results of the joint ERT and seismic surveys were used to detect known voids and probable unknown additional voids. Boreholes drilled in several locations along the survey line were used for verification of the geophysical methods' results. Since the MASW showed a limited ability to accurately resolve the subsurface or the size of underground voids at this specific site, the results of the MASW are discussed first, followed by the results based on the joint use of ERT and SRT.

4.1. MASW survey results

Fig. 3 shows the time traces and the dispersion curve resulting from the processing of the fourth subarray of Line B with a source offset of 6.5 m from start of the array. There is a known void at an approximate distance of 37 m along the line. The time-offset traces in Fig. 3a show a delay in the seismic wave train across the known void location indicating a potential delay in the travel times of various waves to the sensors. However, the size of the observable distortion is significantly smaller than the array length, making this delay only a small portion of the measured data. Arslan et al. (2021) reported that MASW has limitations in accurately resolving subsurface anomalies with certain characteristics. Anomalies with lateral extents smaller than approximately half the length of the geophone array, situated at depths greater than 5 m, are unlikely to be resolved precisely by MASW. This limitation applies even when the anomalies possess considerable thickness (greater than 2 m) and exhibit significant impedance contrasts (greater than 2) compared to the surrounding medium. The findings suggest that caution should be considered when interpreting MASW data for the detection of such anomalies, as their accurate delineation may be compromised by the inherent constraints of the method.

Additionally, the noise interference from the bordering, high-traffic, roadway degraded data quality. Traffic vibrations tend to mask subtle velocity effects, especially given the limited void volume. Moreover, the limited frequency bandwidth and poor dispersion curve quality in Fig. 3b suggests difficulties with extracting interpretable phase velocity frequency behavior for subsequent inversion. Urban background noise commonly overlaps with the low frequency range most sensitive to shallow features (Xu and Butt, 2006). The combination of energy spreading over the array length versus inconsistent noise patterns between sequential source offsets can severely distort coherent dispersion trends. While traffic noise impacts data collection, another challenge is the weak contrast in shear wave velocity between the void and the surrounding weathered rock (Nasseri-Moghaddam et al., 2007). The gradual stiffening of the rock can also lessen the sharpness of the velocity gradient, making it more difficult to identify the void. Considerable prior success imaging voids relies on sharp property changes not necessarily replicated at this site. In summary, the void's small size, noisy setting, subtle subsurface gradients, and dispersion analysis difficulties could collectively explain the inadequate detection. Therefore, no further processing of MASW data was completed for this project.

It should also be noted that MASW is an inherently 1D method: its theoretical development relies on the assumption of a horizontally-layered system that is laterally homogeneous, i.e., there can be no property variability on any horizontal plane. For a subsurface anomaly to be detectable, it would have to be similar to a soil layer, i.e., to have a finite thickness in depth, but extend horizontally to infinity. Though there have been many attempts to use MASW for the detection of finite subsurface anomalies, the violation of its theoretical underpinnings is at the heart of the method's failure to reliably detect the size, shape, and location of such anomalies.

4.2. ERT and SRT survey results

The ERT and SRT results are presented together in this section to allow readers to compare the results more easily. First, the results are provided for a survey line located over the known void encountered at the site. Then, the results are presented for survey lines on each side of the known void, and finally the results are presented for lines away from the known void. At the end, a 3D depiction of the ERT results is presented.

In this study, a consistent interpretation method was employed across all geophysical profiles to ensure uniformity in data analysis and presentation. In the ERT sections, the resistivity values can be broadly interpreted as follows: Regions with ER values approximately less than 200 Ωm are typically classified as either fine-grained soil, soil-filled voids, or fractured zones with water circulation within the karst system. These low resistivity areas may indicate the presence of conductive materials or enhanced fluid flow within the subsurface. On the other hand, ER values approximately greater than 10,000 Ωm are generally associated with air-filled voids or other highly resistive features. The presence of these high resistivity anomalies can be a strong indicator of open, air-filled karst cavities. The intermediate ER values, ranging from roughly 200 Ωm to 10,000 Ωm, have less definitive interpretations in this particular study. This broad range may correspond to a variety of subsurface materials, such as coarse-grained soil, weathered rock, or more competent bedrock. The specific interpretation of these intermediate resistivity zones requires additional context and integration with other geophysical and geological data. The interpretation of ERT data is often site-specific and can be influenced by factors such as the local
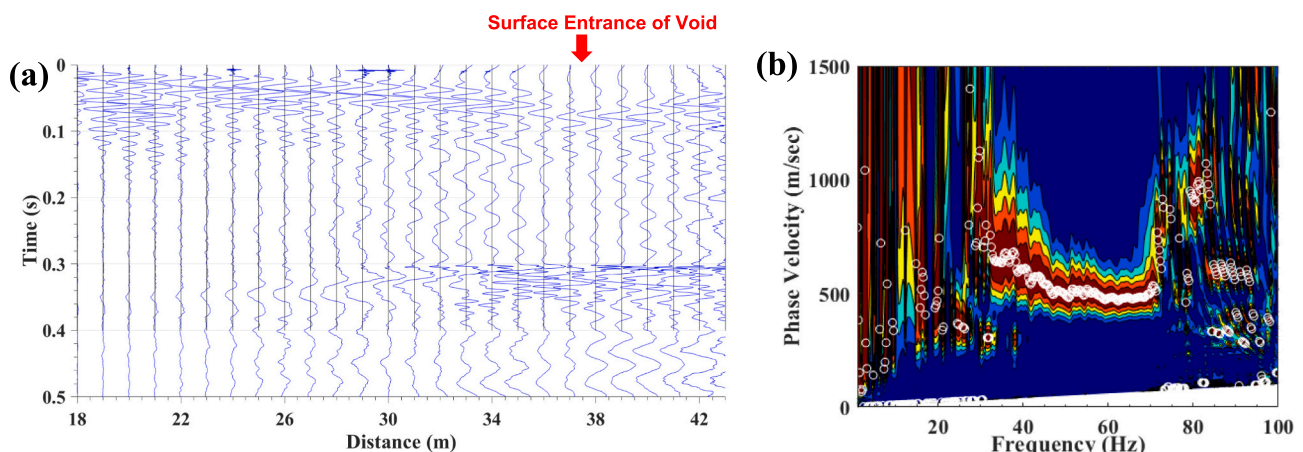

Fig. 3. (a) time trace of forth subarray of Line B (b) dispersion data for same subarray.

geology, hydrogeology, and the nature of the karst features. The resistivity thresholds provided here serve as general guidelines, but the precise delineation of subsurface conditions may vary depending on the unique characteristics of the study area.

This approach was carefully selected based on general principles of ERT interpretation in karst environments, prior to any comparison with borehole data. It's important to note that this study followed a blind methodology, where ERT investigations were conducted and interpreted independently of the borehole data. The borehole logs were obtained subsequently and were not used to calibrate or adjust the ERT model. This blind approach allows for an unbiased assessment of the ERT method's predictive capabilities in karst environments.

The interpretation strategy aims to provide a consistent framework for analyzing the ERT profiles across the entire study area, rather than optimizing for individual profiles or locations. While this approach may result in some localized discrepancies between ERT interpretations and borehole data, it maintains consistency in the presentation of results and demonstrates the strengths and limitations of ERT when applied without prior knowledge of subsurface conditions. The comparison between the independently interpreted ERT results and the borehole data serves to validate the effectiveness of the ERT method and highlight areas where further refinement in interpretation may be needed in future studies.

4.2.1. Geophysical survey over the known void

Fig. 4 illustrates the geophysical survey lines over a known void. Fig. 4a displays the ERT survey Line X with 2 m electrode spacing, which, due to the total array length, provided greater penetration depth for, potentially, identifying deeper anomalies. In contrast, Fig. 4b offers a higher resolution ERT image of the subsurface conditions at a shallower depth in proximity to the known void. There are multiple boreholes logs available to corroborate the 2D resistivity sections along these two survey lines. Fig. 4c shows an SRT image of the same location; its origin is the same as that of Lines X and B. The color-coded electrical resistivity scale for the ERT sections, and the P-wave velocity scale for the SRT section are shown next to the sections. The alignment of Line B (Fig. 4b) with Line X (Fig. 4a) is depicted with a black trapezoid on the

Line X survey section. The surface entrance of the void and the boring logs, accompanied by a material index, are also depicted in all three sections.

The bedrock depth appears very shallow, situated at approximately 1 m depth according to the ERT and SRT images, although it is resolved at a deeper depth in Cross Section X due to the lower resolution of the line. The increased electrode spacing in Line X enabled deeper penetration, while compromising the resolution near the surface. Consequently, the lower resistivity zone appears more accurately delineated in Line B compared to Line X, as also corroborated by the boring logs. The shallow soil layer, based on the borehole, consisted of brown, fine to medium grained, dry to moist clayey sand, mixed with light gray limestone fragments. This layer was resolved with low resistivity (<100 Ωm) and low velocity (<600 m/s). According to the boring logs the bedrock was composed of soft to very hard, vuggy limestone rock, experiencing slightly to highly fractured conditions. The resistivity of the bedrock ranges from 400 to 900 Ωm in Line B, while varying between 400 and 1200 Ωm in Line X. This represents up to a 30 % difference in some areas, attributed to the differing resolution levels. However, this resistivity range shows an overall agreement with values reported for fractured limestone in the literature, generally falling between 450 and 2000 Ωm (Robert et al., 2011). The end of Line X (60 m to the end) corresponds to the start of a large wall at the site, as shown in the Google Earth image in Fig. 2. The presence of the wall led to survey measurement errors for the end portion of Line X.

Two major areas of interest are delineated on the cross sections as resistivity anomalies, displaying high- and low-resistivity contrasts annotated as EX1, EX2 in Line X and EB1, EB2 in Line B at distances of approximately 33 m and 40 m along the line, respectively. The locations of these two anomalies are approximately similar for both survey lines, but appear more pronounced in Line X. The low-resistivity zones EX2 and EB2 exhibit resistivity values below 200 Ωm. In contrast, the high-resistivity anomalies EX1 and EB1 show values exceeding 2000 Ωm in Line X and 10,000 Ωm in Line B, respectively. This discrepancy in resistivity magnitudes likely stems from the smoothing effect during the inversion process, which aims to avoid sharp resistivity contrasts. The
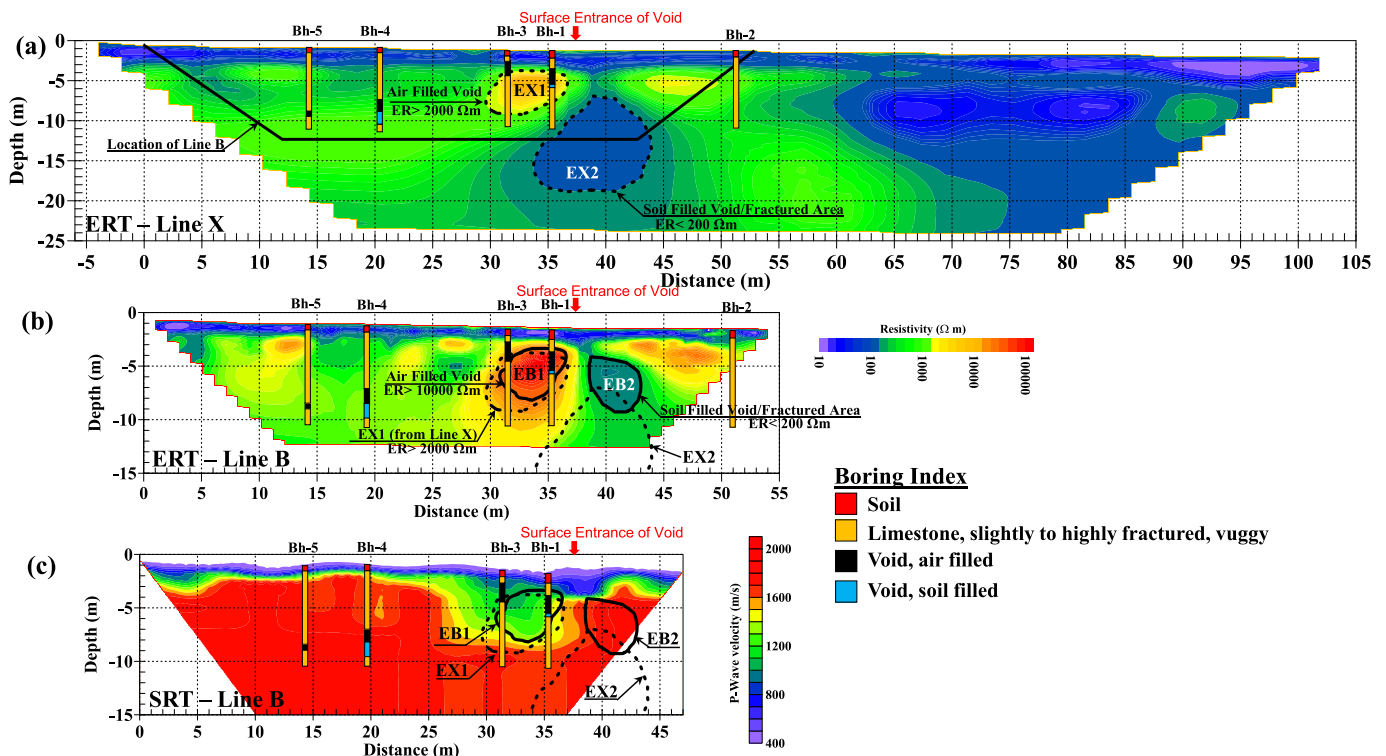

Fig. 4. Geophysical survey through known void (a) ERT line X (2 m electrode spacing), (b) ERT line B (1 m electrode spacing) and (c) SRT line B.

greater electrode spacing in Line X yields a more homogeneous resistivity distribution (Giao et al., 2003; Robert et al., 2011). This also affects the dimensions of the anomaly, with a more pronounced high-resistivity feature EX1 to EB1 at 33 m distance and a more extensive low-resistivity zone EX2 compared to EB2 at 40 m distance. The smoothing effect in the ERT inversion occurs because the inversion process attempts to produce a model with smooth resistivity variations rather than producing sharp interface boundaries between different resistivity zones. This is implemented by adding a regularization term to the inversion's Lagrangian functional that promotes the spatially smooth resistivity distributions. The impact of smoothing is particularly noticeable when using electrode configurations with greater spacing, effectively reducing the resulting resolution. With increased electrode spacing, the inversion redistributes anomalous resistivity values over a larger volume, thereby decreasing the magnitude of extremes and leading to the merging of anomalies (Loke et al., 2013).

The high-resistivity anomaly EB1 is situated proximal to the known void entrance and aligns with the void encountered in boring logs Bh-1 and Bh-3. However, minor differences exist between the void depth and position in the ERT section compared to the boring logs. This high-resistivity zone delineates the lateral extent of the air-filled void intersected by the boreholes. However, the boreholes generally encountered the void at a higher elevation than observed on the ERT sections. The low-resistivity region EB2, located approximately 40 m along the line, with a resistivity of less than 200 Ωm in both sections may represent either a partially soil-filled void or a fractured zone with water circulation within the karst system. While the resistivity of this zone is consistent with the clayey sand resolved near the surface, lack of a clear low velocity signature in the SRT profile suggests it may not be a completely soil-filled void. An alternative interpretation is that this zone corresponds to a fractured area with enhanced water flow within the karst network. Further investigation, such as Induced Polarization (IP) surveys, may be beneficial in determining the presence and nature of any infilling materials in this region.

Conversely, no void indications manifest in the resistivity sections near the locations of the additional voids encountered in boreholes Bh-4 and Bh-5, situated approximately 20 m and 15 m along the line. As shown in the literature, voids can exhibit approximately the same resistivity as the surrounding rock in some scenarios. One possible explanation is that the voids may be too small relative to the depth (~10 m) where the voids are observed (Martinez-Moreno et al., 2014). In this case, small-scale heterogeneities are masked by the inherent volume averaging effect in ERT, which smooths out localized irregularities during inversion. Another potential explanation is the shadowing effect of the resistive rock mass. Shadowing happens when an anomaly is positioned below an extensive body of high- or low-resistivity material, concealing underlying features (Chalikakis et al., 2011; Kaufmann et al., 2012). Therefore, the deeper anomaly is obscured by shallow features with very high- or low-resistivity contrast. Shadowing is most problematic when imaging targets situated under extensive resistive terrain, such as competent rock, which causes current flow to be dominantly controlled by the overlying resistive layer, hiding subtler variations below. The ability to resolve deeper features relies on the resistivity contrast and thickness of the overburden relative to the target (Dahlin and Loke, 1998).

The location of the resistivity anomalies EX1-EX2 in Line X and EB1-EB2 in Line B are depicted on the SRT section in Fig. 4c. The SRT section successfully resolved the void location between 26 and 37 m distance along the line, matching the position indicated by boreholes Bh-1 and Bh-3, corresponding to the EX1/EB1. Although the right boundary of the SRT-resolved void aligns with EX1/EB1, a discrepancy exists for the left boundary, where the SRT section shows a more pronounced area. This discrepancy could arise from the different physical properties measured by ERT (electrical resistivity) and SRT (P-wave velocity). While ERT may not detect variations within a homogeneous zone, SRT can resolve localized velocity changes, leading to potential differences in the delineated anomaly boundaries. The void is delineated as a zone of low P-wave velocity (<1000 m/s) compared to the surrounding rock medium, which exhibits velocity more than 1500 m/s. Notably, this reduced velocity zone appears more extensive in the SRT section than the respective ERT anomalies, potentially delivering an increased interpreted void area. SRT relies on the detection of first-arrival travel times and raytracing to map velocity distributions, with the assumption that sufficient rays penetrate into all model regions. However, voids often violate these assumptions, presenting a challenge for accurate velocity characterization in which the inverted velocity is only a little lower than the surrounding volume (Sheehan et al., 2005). Air-filled voids exhibit low-velocity spots. However, recovered void velocities from SRT inversions are often much higher. This velocity overestimation stems from inadequate ray coverage through voids. The inversion underestimates the velocity reduction and distributes higher surrounding velocity into the void space. This could be the reason for the larger void in the case of SRT compared to ERT. Complex void geometry can further hinder velocity resolution, as a void's shape affects wave propagation and refraction. Overall, despite inaccuracies in the absolute P-wave velocity within the void space, SRT successfully delineated the location of the major void evident near the ground surface, annotated by anomalies EX1/EB1 in resistivity sections. The void position shows good agreement between the SRT and ERT results. However, the SRT survey was unable to definitively resolve the soil-filled void/fractured zone annotated as EX2/EB2 identified in the resistivity sections. The SRT likely resolves the partially soil-filled void/fractured zones identified in the ERT as rock medium. There is minimal P-wave velocity contrast between the soil-filled sections and fractured rock encountered in the borings, so SRT is unable to differentiate these two void types like ERT, which resolves them with distinct resistivity values.

The joint application of ERT and SRT provides complementary information crucial for comprehensive void characterization. ERT accurately delineates resistivity contrasts associated with air- and soil-filled voids/fractured zones, enabling differentiation based on their distinct signatures. Conversely, SRT offers an integrated perspective on the overall void geometry and continuity by mapping velocity distributions. By combining these complementary datasets, a more robust and reliable characterization of the subsurface void network can be achieved, enhancing the effectiveness of detection and remediation efforts. The differences between ERT and SRT in the detection of air-filled and soil-filled voids highlights the relative strengths of each geophysical method. While ERT can differentiate air-filled and soil-filled voids based on their distinct resistivity signatures, SRT is better suited for delineating overall void extents, but may struggle to distinguish void infill types without significant velocity contrasts. The combined interpretation of ERT and SRT data leverages the strengths of each technique, providing a more comprehensive understanding of subsurface conditions.

Similar to the ERT sections, the dimensions of the void are slightly exaggerated within the SRT image. The smoothing effect of the tomography process distributes the velocity anomaly over a broader area, enlarging the perceived size (Sheehan et al., 2005). Nonetheless, the SRT provides reliable detection and lateral positioning of the void due to strong velocity contrast. No distinct void signature is visible in the SRT section near boreholes Bh-4 and Bh-5 from 15 to 20 m distance. This aligns with the ERT results and can again be attributed to the combined effects of small void size and shadowing (Chalikakis et al., 2011). Low-velocity zones beneath high-velocity layers are especially problematic, as refractions may not sample the deeper void. The resolution limits of SRT and the masking influence of high-velocity surface layers obscure identification of these deeper, smaller voids. Specifically, the P-wave refraction method shows reduced sensitivity against low-velocity anomalies situated below high-velocity strata, as the refracted first arrivals are controlled by the overlying high-velocity layer.

A factor limiting detection of deeper voids in bedrock is insufficient ray coverage below the overburden interface, as demonstrated by Sheehan et al. (2005) in a forward model with a sharp velocity contrast

and no gradient within the bedrock layer. With no rays penetrating below this interface, voids situated at depth in the bedrock cannot be resolved. However, using velocity gradients and less extreme contrasts between the overburden and bedrock would allow deeper penetrating rays to detect underlying voids. For rays to effectively sample deeper targets, they must have a pathway to refract back to the surface, either via velocity changes under the void or small vertical gradients in the surrounding material. This concept is demonstrated through the ray-tracing of Line B shown in Fig. 5. For the larger, shallower void on the right side of the section, some rays penetrate below the void, enabling its detection. However, for the smaller, deeper void situated in the more homogeneous bedrock velocity, no rays sample beneath the void. The lack of rays refracting underneath this deeper void prevents its resolution. Variable bedrock velocity and sufficient ray penetration depth below a void are key factors controlling its detectability with SRT. In summary, while ERT provides enhanced resolution of void composition based on resistivity variations, SRT complements the investigation by clearly defining the lateral void extent through velocity reductions. Using both techniques in tandem provides more robust void characterization than either method alone.

4.2.2. Geophysical surveys close to the known void

The ERT and SRT images in Fig. 6 and Fig. 7 on each side of the known void, provide complementary information. Fig. 6a displays the ERT survey Line A with 1 m electrode spacing and Fig. 6b shows an SRT image of the same survey line. Both sections resolve a thin near-surface layer of low resistivity (<100 Ωm) and low velocity (<500 m/s) indicative of soil overburden. This overlies more competent limestone bedrock with moderate resistivity (100–1500 Ωm) and velocity (>1500 m/s). At 34 m distance, a distinct high-resistivity anomaly (>10,000 Ωm), annotated as EA1, was detected. This anomaly corresponds to a zone of lower seismic velocity (<1200 m/s).

However, the low velocity zone observed in the SRT profile is more extensive and stretched leftward compared to the high resistivity

anomaly EA1 in the ERT data. This discrepancy in the lateral extent of the void signature between the two methods is an important consideration. Borehole Bh-1 intersected an air-filled void at this location between 3 and 5 m depth, confirming the geophysical interpretation. The location of the resistivity anomaly EA1 is relatively well matched with the air-filled void, although the anomaly EA1 extended to a deeper depth compared to the borehole data.

The differences in the observed dimensions of the void feature between the ERT and SRT methods can be attributed to several factors. Firstly, the fundamental principles and sensitivities of the two techniques are inherently different. The resistivity method is primarily sensitive to changes in the electrical properties of the subsurface, while the seismic method responds to variations in acoustic velocities. These distinct physical responses can lead to differences in the perceived size and shape of the void. Additionally, the inversion and imaging algorithms used to process the ERT and SRT data can also influence the final representation of the subsurface features.

Furthermore, the void in question is a complex 3D structure, but the geophysical surveys were conducted in 2D. Attempting to model a 3D feature using 2D techniques can result in distortions and potential misalignments between the two data sets. The discrepancy between the depth of the void from the ERT and SRT surveys could also be attributed to differences in how the respective methods resolve the properties of the void infill material. While the ERT section may have captured the resistivity of the infill close to the void itself, the SRT section may have been more sensitive to the acoustic properties of the surrounding bedrock.

Additional isolated resistivity peaks at 15 m and 47 m distance may indicate smaller voids or fractures; however, the SRT shows no corresponding velocity reductions. This discrepancy highlights differences in anomaly sensitivity and resolution limits between the two methods. Minor resistivity decreases in ERT could stem from subtle weathering or water content changes undetectable in the velocity field (Shevnin et al., 2007). The lack of a void in Bh-2 supports the latter explanation, despite
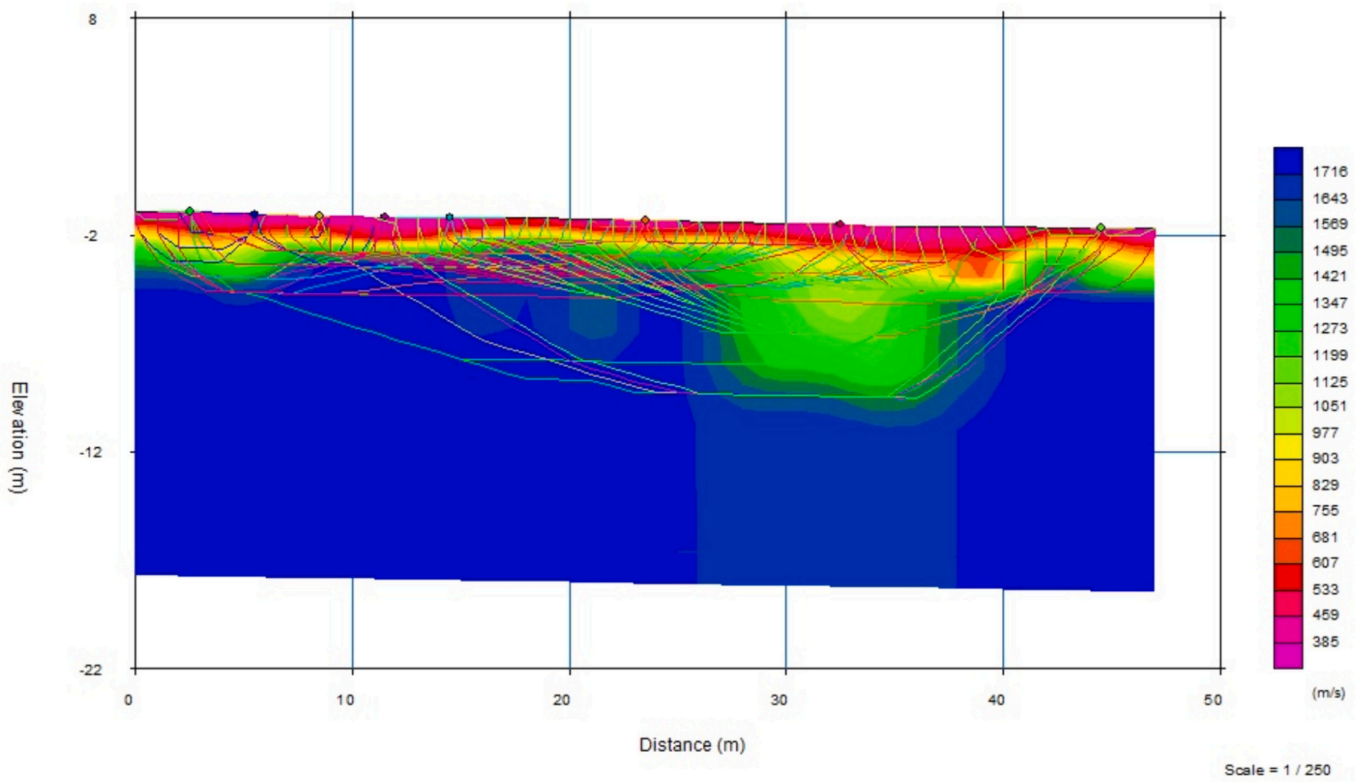

Fig. 5. P-wave raytracing of line B, shown in the P-wave refraction analysis software (Plotrefa).
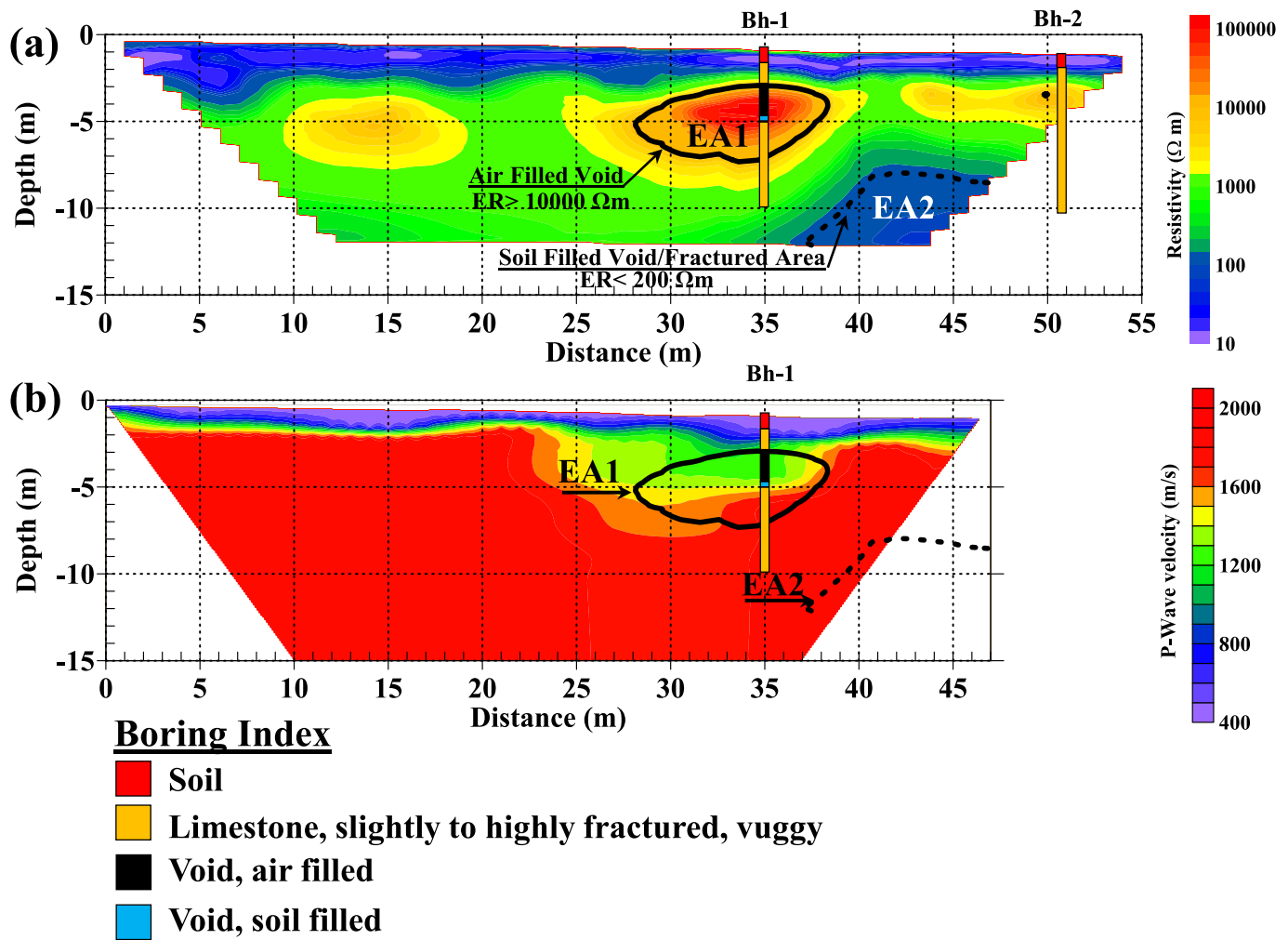
Fig. 6. Geophysical survey of line A close to known void (a) ERT survey and (c) SRT survey.

the local ERT variation.

A low resistivity zone annotated as EA2 observed at approximately 42.5 m distance on ERT profile. A similar low resistivity zone was observed at the same distance along profiles B and X. However, as this low resistivity feature is located closer to the edge of section A, there is less confidence in its interpretation. The EA2 anomaly may represent either a soil-filled void or a zone of fractured and water-bearing karst. The relatively high resistivity values of around 100–200 Ωm may not be consistent with what would be expected for a void infilled with clay-rich sediments, which typically exhibit resistivities below 50 Ωm. Therefore, an alternative interpretation is that EA2 corresponds to a fractured area within the karst system, with enhanced groundwater circulation.

It is worth noting that the SRT section is only 46 m long; therefore, the low resistivity zone EA2 observed in the ERT data lies outside of the ray coverage of the SRT profile. This limited overlap between the two datasets at the location of EA2 likely contributed to the absence of a clear low velocity signature associated with this feature. In addition, the inherent challenge of accurately modeling a 3D void feature using a 2D geophysical technique precludes precisely resolving the true shape and dimensions of such a complex subsurface structure.

Shown in Fig. 7 is the ERT and SRT profile of Line C located in the opposite side of the Line A. Similar to two previous sections there is a shallow soil layer overlying a more competent rock. The ERT and SRT images of Line C in Fig. 7, located near to the known void on the opposite side of Line A, provide additional void characterization, with some variations from Line A. As before, a thin low-resistivity (<100 Ωm) and low-velocity (<500 m/s) layer represents soil overburden, underlain by

fractured limestone bedrock. A distinct high-resistivity (>10,000 Ωm) anomaly annotated as EC1, situated at 34 m distance, aligns with the low-velocity void signature in SRT after 32 m distance to the end of line. However, the high-resistivity area appears much smaller than the air-filled voids in Lines A-B. This suggests either partial infilling or the presence of the void boundary at this location across the intersecting line. The bottom depth of the high-resistivity zone EC1 at a distance of 34 m maches with the bottom boundary of the low velocity area in SRT sections. In addition, the bottom depth of the void discovered in Bh-3 at the distance of 31 m matches very well the bottom depth of the low-velocity zone in SRT section. However, the 4–7 m depth in the ERT section exceeds the 2.5–4.5 m depth of the void logged in Bh-3. Smoothing effects during ERT inversion can displace the resistivity anomaly downward when sharp property contrasts occur (Loke et al., 2003), while velocity reductions manifest at the actual void elevation. Another explanation stems from variations in void geometry, where the irregular shape may cause the anomaly to manifest at different positions across intersecting survey lines (Grandjean and Leparoux, 2004). Complex voids violate the 2D assumptions of both methods making the locations of the resolved void less reliable. SRT relies on having enough raypath coverage to accurately sample the anomaly. However, in rock media with low-velocity gradients, there may be insufficient raypaths penetrating the deeper extent below the anomaly. As a result, the recovered velocity map tends to have smoother gradients compared to the resistivity extremes present in the ERT map.

In contarst to Line B/X the low-resistivity region annotated as EC2 at 41 m distance aligns with lower velocities in SRT, likely indicating a soil-
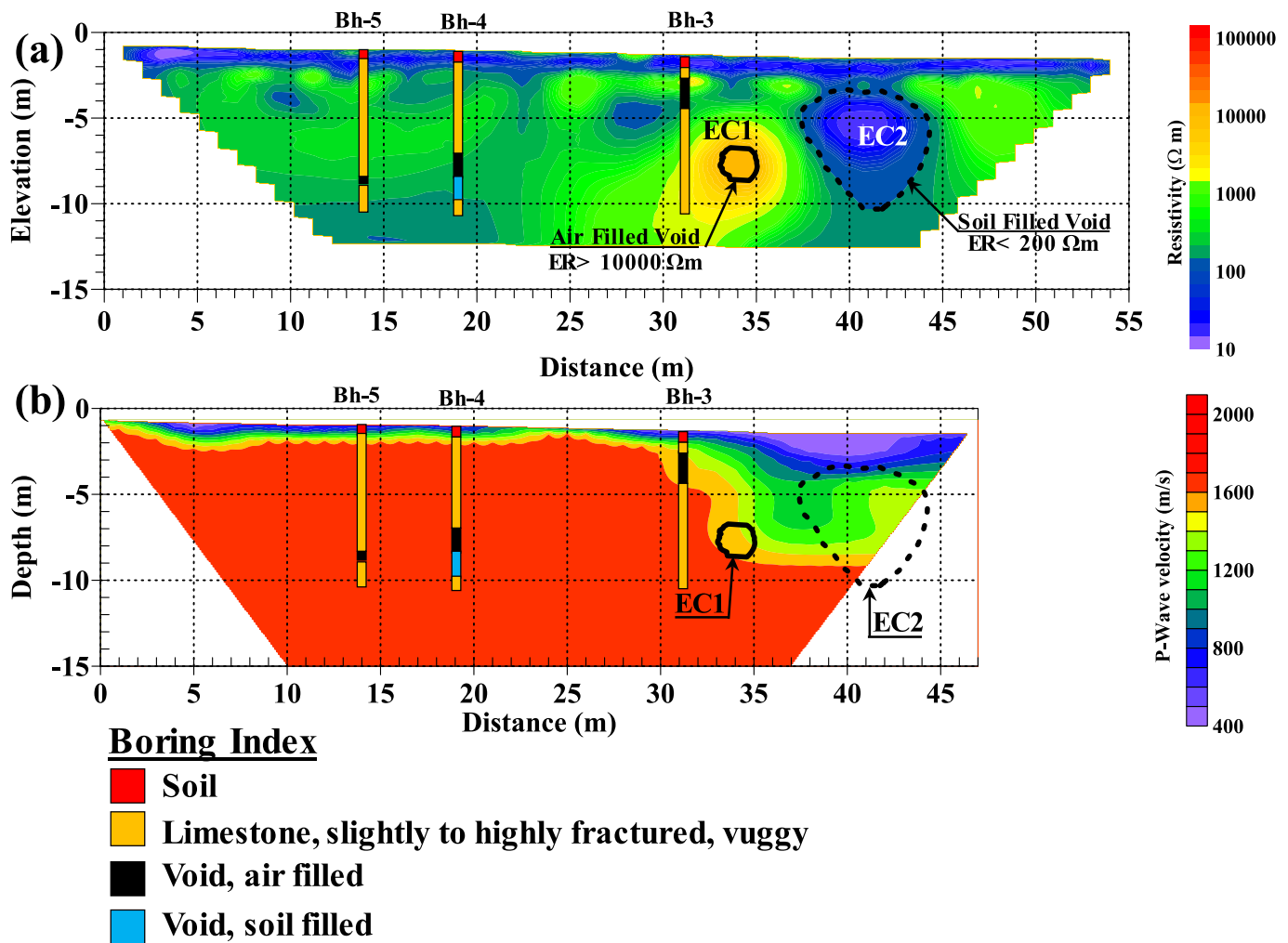
Fig. 7. Geophysical survey of line C close to known void (a) ERT survey and (c) SRT survey.

infilled void not visible at the surface. However, artifacts can occur near metal utility crossings causing distortions, as is the case with the valve at 35 m. Deeper voids in Bh-4 and Bh-5 remain undetected, as previously discussed. The surrounding competent rock material, characterized by higher velocities, wouldn't allow rays to sample these deeper anomalies, while the small size makes resistivity-based detection difficult.

4.2.3. Geophysical surveys away from the known void

The surveys in Fig. 8 and Fig. 9 show regions without verified voids, providing background site characterization away from the known void. As observed in previous lines, a thin soil layer is underlain by more resistive and faster velocity limestone bedrock. However, there is no distinct high-resistivity (>10,000 Ωm) anomalies indicative of a large air-filled void across these profiles. Several isolated low-resistivity (<150 Ωm) zones exist in the ERT sections at 41 m distance on line D and within the first 22 m on line G. As resistivities match those for soil, these could denote infilled voids, although artifacts frequently occur near metal utility elements like the metal pipes and valves present along the lines at distance of 35 m of line D and at first 10 m of line G (Yi et al., 2001; Porsani et al., 2004). Current distortion from such conductors presents measurement variations unrelated to geology. Notice that the SRT sections in Fig. 8b and Fig. 9b lack corresponding velocity reductions in these anomaly areas. As SRT proves more robust against utility interference, this suggests the ERT variations stem from utility rather than subsurface voids. Additionally, gradual property changes make resolving small-scale, low-resistivity, features challenging

(Kaufmann et al., 2012). The absence of voids aligns with moving away from the mapped extent of the known karstic feature. As the complementary SRT data detects no velocity anomalies indicative of voids, the isolated ERT distortions likely reflect artifacts. However, confirmation would require invasive testing.

4.2.4. Pseudo-3D ERT

Pseudo-3D geophysical modeling has grown in popularity due to its ability to map subsurface volumes compared to individual 2D planar sections. Combining multiple interpolated 2D datasets enables approximating 3D volumes, improving spatial delineation of anomalies not discernible within 2D profiles (Papadopoulos et al., 2007; Loke et al., 2013).

The pseudo-3D model in Fig. 10 maps three prominent high-resistivity (>50,000 Ωm) anomalies indicating suspected air-filled voids. These manifest beneath lines A-C at depths of 2–6 m, matching void positions identified on individual 2D sections. Fig. 11 highlights an extensive interconnected low-resistivity (<125 Ωm) zone from 37 to 47 m distance under lines B-E, likely representing soil-infilled cavities/fractured zones starting at 1–2 m from the near surface soil layer and extend to 8–10 m below the surface depth representing either soil-filled voids or artifacts due to utility crossing. These align with the potential soil-filled void features observed across sequential 2D profiles. Other isolated low-resistivity regions observed on the 2D lines are not observed in the pusedo 3D results suggesting possible infrastructure artifacts as supported by the SRT analysis that lacked corresponding
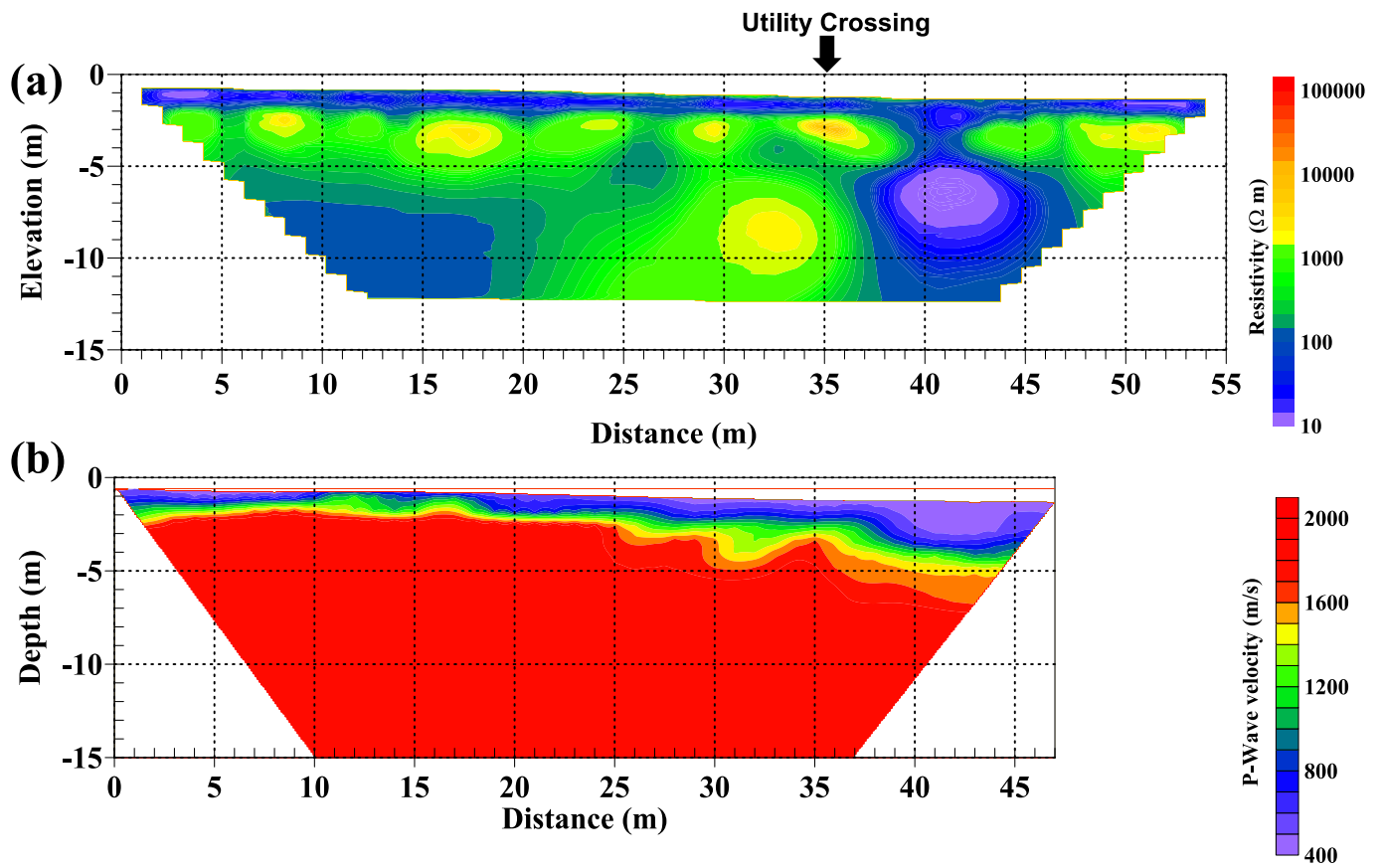
Fig. 8. Geophysical survey of line D away from known void (a) ERT survey and (c) SRT survey.
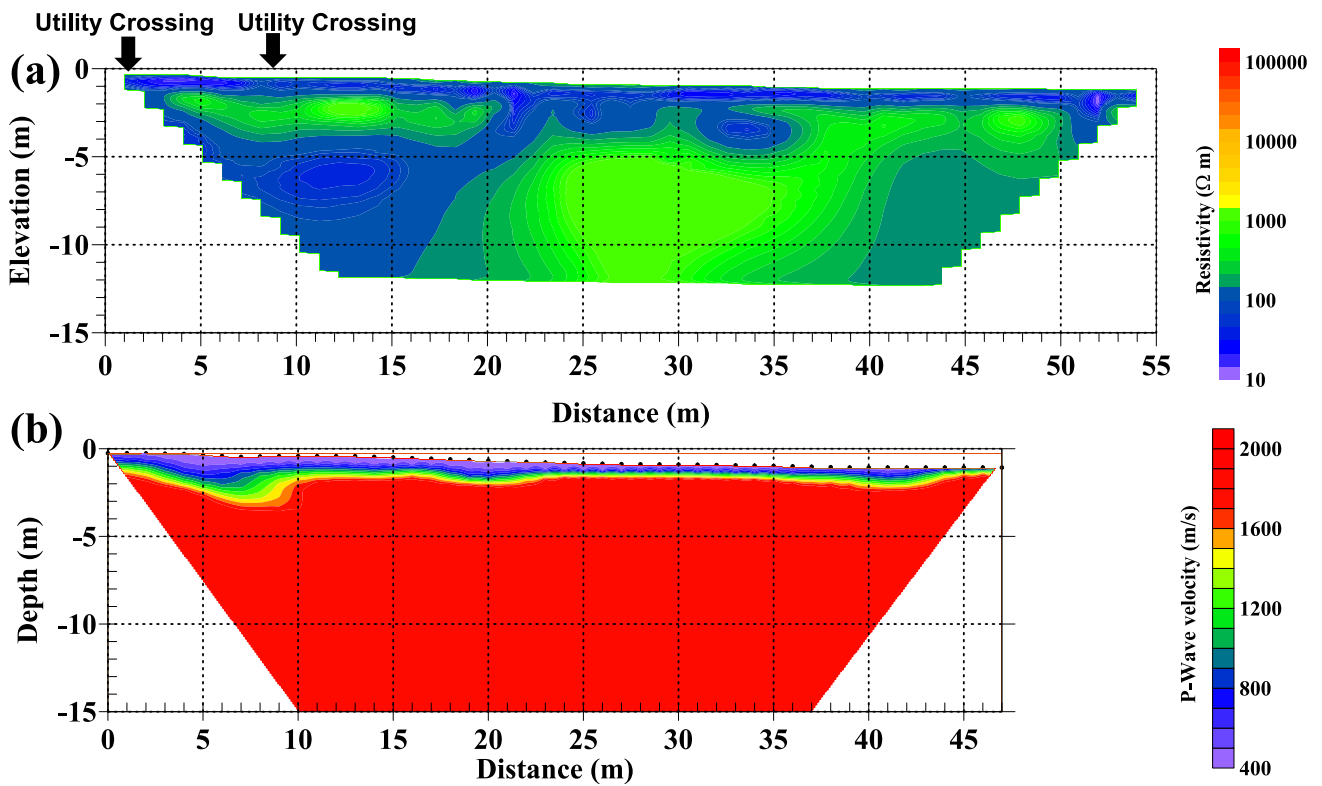

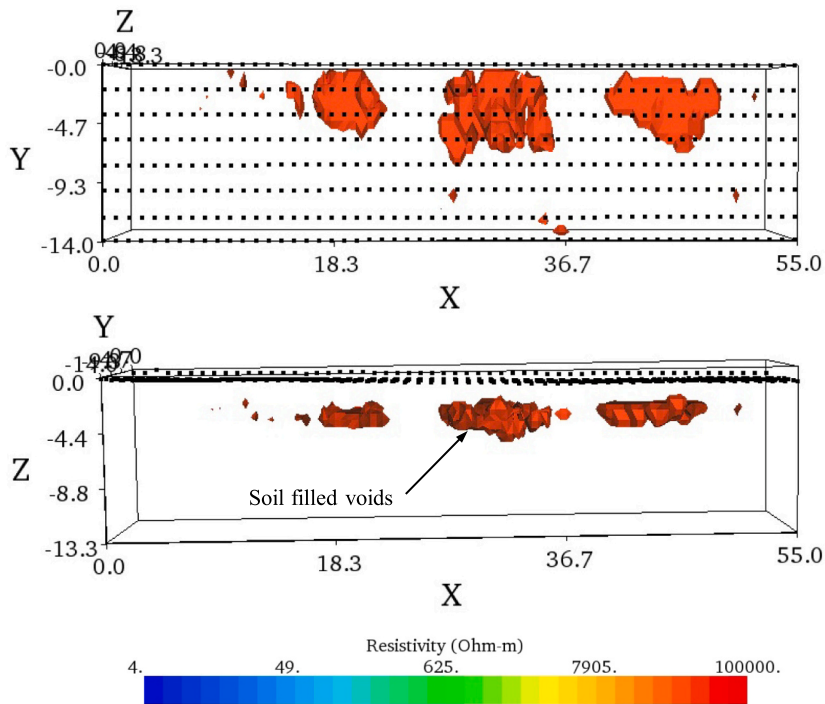**Fig. 9.** Geophysical survey of line G away from known void (a) ERT survey and (c) SRT survey.

Fig. 10. Pseudo 3D resistivity model with high-resistivity (>50,000 Ω-m) areas of possible air-filled voids highlighted. The top figure is the top view and bottom figure is the profile view looking North.
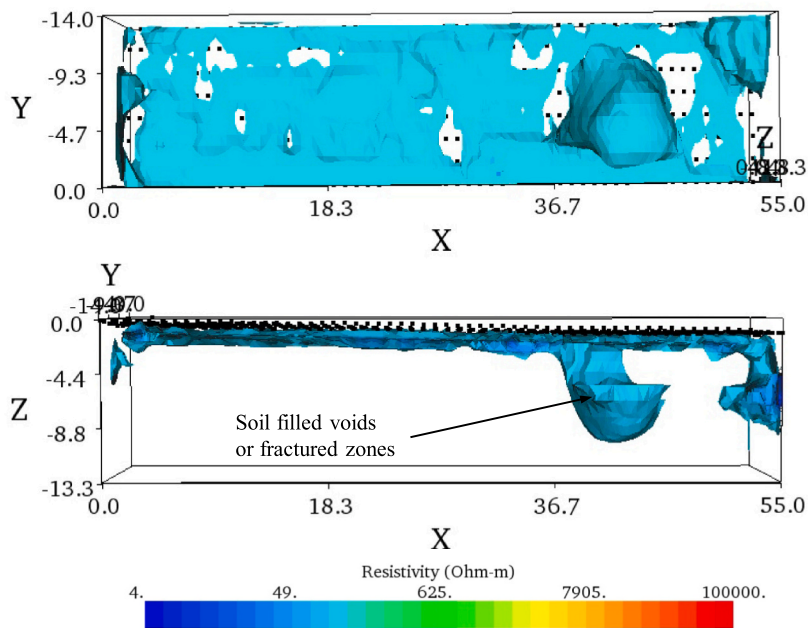

Fig. 11. Pseudo 3D resistivity model with low-resistivity (<125 Ω-m) areas of possible soil-filled voids/fractured zones highlighted. The top figure is the bottom view and bottom figure is the profile view looking North.

anomalies.

The link between resistivity anomalies across the width of the volume reaffirms possible void connectivity that is not discernible from the 2D sections. However, the 3D interpolation cannot resolve finer details, which were obscured even in the original 2D ERT profiles. Complementary methods like 3D SRT and/or invasive testing could enhance the imaging. Nonetheless, the pseudo-3D ERT models provide improved

context guiding remediation decisions relative to the more isolated 2D data.

5. Discussion

The study results highlighted the promise, but also the limitations of using non-invasive geophysical imaging techniques for void detection.

The MASW results demonstrated the inherent constraints in the methodology that prevent reliable imaging of finite-size heterogeneities, including subsurface voids. MASW's theoretical assumptions fundamentally limit the ability to resolve anything but very large anomalies. The presence of noise can also severely contaminate the dispersion analysis critical for inversion. These factors help explain MASW's inability to detect and localize the subsurface voids in this study.

The study results also demonstrated the promise of using ERT and SRT jointly for void detection. Key findings demonstrated that ERT and SRT can successfully identify subsurface voids under relatively favorable conditions. It is noted that detectability improves when the two methods are used jointly, over the detectability resulting from the use of each method on its own. However, detectability proved sensitive to site-specific factors. Small or irregular voids may evade detection depending on geometry and property spatial gradients. Deeper voids may fall outside the resolution and detectability limits of both methods. Heterogeneous surrounding material can mask subtle resistivity or velocity signatures indicative of voids. Preexisting utilities likewise interfere with measurements, producing artifacts that complicate interpretation.

The ERT results revealed the presence of both high- and low-resistivity anomalous zones, indicative of air- and soil-filled voids/fractured zones, respectively. Simultaneously, SRT effectively delineated the overall extent of the void area but was unable to resolve the internal characteristics of the void infill material. By integrating these complementary datasets, a more complete picture emerged, characterizing not only the locations and geometries of voids, but also offering insights into their potential infill states. The joint ERT-SRT approach demonstrated the value of multi-method geophysical investigations for complex subsurface targets. Each technique contributes unique information that can be synthesized to enhance the interpretation capabilities beyond what is achievable with a single method alone. This combined strategy is particularly powerful for hazard assessment and risk mitigation in areas prone to subsidence and sinkhole formation.

These variable outcomes align with the mixed results reported in other field site investigations in the literature. No single imaging technique can conclusively confirm a void. Findings depend greatly on array parameters selected during field deployment, and the parameterization of the computational inversion processes. Users cannot exhaustively sample the entire method sensitivity range at an unknown site, to ascertain detection of voids of any size and at any depth. Success also hinges on the specific environmental setting, target depth, size, infill material, and geologic variability impacting property contrasts. These factors currently preclude the replacement of invasive investigations with noninvasive imaging for critical infrastructure projects.

At present, geophysical methods provide a useful guide for optimizing subsequent invasive testing locations through selective anomaly targeting. But validation drilling remains necessary to prove actual void existence. Ideally, future work should implement standardized assessment procedures across different sites using consistent processing workflows. This would help quantify the range of conditions enabling reliable detection for each method. Additional datasets and case studies are critical to refine technique limitations toward transitioning noninvasive imaging into primary site characterization tools.

6. Conclusion

Based on the geophysical testing results and boring information thus far, the following conclusions can be drawn:

- While no single method stands out as the optimal approach for detecting subsurface anomalies, whether soil-filled, water-filled, or air-filled (voids), ERT demonstrates enhanced capabilities under typical site conditions.
- For all methods, their ability to detect an anomaly of a given size depends on the method's parameters during field deployment (sensor spacing, source and sensor characteristics, etc.), as well as on

the local site conditions (presence of water in the deposits, orientation, anomaly shape and size, etc.).
- Since during a blind field investigation, it is not possible to sweep over the entire parameter space (i.e., conduct ERT surveys using different array lengths, and multiple electrode spacings, etc.), it is quite possible that a few subsurface anomalies will be detected while others might be missed. If available, site-specific a priori information, can assist in partially alleviating such difficulties.
- The ERT method, especially in the context of 3D surveys, is promising, but not without potential pitfalls.
- The MASW method appears to have limited ability to accurately resolve either the location or the size of subsurface anomalies, or both, unless they are located close to the surface and are of considerable size. The difficulty is rooted in MASW's theoretical underpinnings which do not allow consideration of arbitrary heterogeneity – a necessity when interested in the detection of subsurface anomalies.
- Although SRT detects voids through significant velocity decreases, care must be taken in interpreting the magnitude of reduction. Integrating SRT with, advanced imaging approaches such as full waveform inversions may improve velocity accuracy. But intrinsic challenges remain for SRT in accurately defining velocities within void spaces. An integrated geophysical approach is recommended, with SRT providing void/anomaly presence and approximate extent, while other methods help determine the anomaly's physical properties.

In summary, while geophysical imaging shows promise for noninvasive void identification, continued validation and technique refinement is needed before these methods can graduate to becoming the primary subsurface site characterization tools, replacing invasive approaches. No single approach detected all documented voids at this complex field site. Outcomes varied based on target depth, size, geometry, property contrasts, surrounding gradients, and field parameters. Using ERT and SRT together enhanced void detection through complementary property sensitivities. But invasive testing remains necessary to prove void existence and precise attributes undeterminable from anomalies alone. Considerable case study aggregation is still required to standardize processing workflows and quantify reliable detection thresholds across different environmental conditions. For now, integrated geophysical interpretation and corroborative exploration provides the most robust site assessment strategy.

CRediT authorship contribution statement

M. Rahimi: Writing – original draft, Visualization, Validation. **C.M. Wood:** Conceptualization, Methodology, Validation, Investigation, Resources, Writing – review & editing, Supervision. **Loukas F. Kallivokas:** Project administration, Investigation, Funding acquisition, Data curation, Conceptualization.

Declaration of competing interest

Data availability

Data will be made available on request.

References

Argote, D.L., Tejero-Andrade, A., Cárdenas-Soto, M., Cifuentes-Nava, G., Chávez, R.E., Hernández-Quintero, E., Garcia-Serrano, A., Ortega, V., 2020. Designing the underworld in Teotihuacan: Cave detection beneath the moon pyramid by ERT and ANT surveys. J. Archaeol. Sci. 118, 105141 https://doi.org/10.1016/j.jas.2020.105141.

Arjwech, R., Ruansorn, T., Schulmeister, M., Everett, M.E., Thitimakorn, T., Pondthai, P., Somchat, K., 2021. Protection of electricity transmission infrastructure from sinkhole hazard based on electrical resistivity tomography. Eng. Geol. 293, 106318 https://doi.org/10.1016/j.enggeo.2021.106318.

Arslan, U., Crocker, J.A., Vantassel, J.P., Cox, B.R., 2021. Ability of the Multichannel Analysis of Surface Waves Method to Resolve Subsurface Anomalies, 2021. IFCEE, pp. 360–371. https://doi.org/10.1061/9780784483428.03.

ASTM International, 2018. Standard guide for using the seismic refraction method for subsurface investigation. In: ASTM D5777, ASTM International, West Conshohocken, PA, United States. https://doi.org/10.1520/D5777-18.

Bharti, A.K., Pal, S.K., Priyam, P., Pathak, V.K., Kumar, R., Ranjan, S.K., 2016. Detection of illegal mine voids using electrical resistivity tomography: the case-study of Raniganj coalfield (India). Eng. Geol. 213, 120–132. https://doi.org/10.1016/j.enggeo.2016.09.004.

Chalikakis, K., Plagnes, V., Guerin, R., Valois, R., Bosch, F.P., 2011. Contribution of geophysical methods to karst-system exploration: an overview. Hydrogeol. J. 19 (6), 1169. https://doi.org/10.1007/s10040-011-0746-x.

Dahlin, T., Loke, M.H., 1998. Resolution of 2D Wenner resistivity imaging as assessed by numerical modelling. J. Appl. Geophys. 38 (4), 237–249. https://doi.org/10.1016/S0926-9851(97)00030-X.

Deiana, R., Bonetto, J., Mazzariol, A., 2018. Integrated electrical resistivity tomography and ground penetrating radar measurements applied to tomb detection. Surv. Geophys. 39 (6), 1081–1105. https://doi.org/10.1007/s10712-018-9495-x.

Diallo, M.C., Cheng, L.Z., Chouteau, M., Rosa, E., Liu, C., Abbassi, B., Dimech, A., 2023. Abandoned old mine excavation detection by Electrical Resistivity Tomography. Eng. Geol. 320, 107123 https://doi.org/10.1016/j.enggeo.2023.107123.

Dobecki, T.L., Upchurch, S.B., 2006. Geophysical applications to detect sinkholes and ground subsidence. Lead. Edge 25 (3), 336–341. https://doi.org/10.1190/1.2184102.

Giao, P.H., Chung, S.G., Kim, D.Y., Tanaka, H., 2003. Electric imaging and laboratory resistivity testing for geotechnical investigation of Pusan clay deposits. J. Appl. Geophys. 52 (4), 157–175. https://doi.org/10.1016/S0926-9851(03)00002-8.

Grandjean, G., Leparoux, D., 2004. The potential of seismic methods for detecting cavities and buried objects: experimentation at a test site. J. Appl. Geophys. 56 (2), 93–106. https://doi.org/10.1190/1.9781560803188.

Howard, A.D., 1964. Processes of limestone cave development. Int. J. Speleol. 1 (1), 47–65. https://doi.org/10.5038/1827-806X.1.1.8.

Hunt, B.B., Smith, B.A., Adams, M.T., Hiers, S.E., Brown, P.E., 2013. Cover-collapse sinkhole development in the cretaceous Edwards limestone, Central Texas. In: 13th Sinkhole Conference. University of South Florida.

Jabrane, O., Martinez-Pagan, P., Martinez-Segura, M.A., Alcalá, F.J., El Azzab, D., Vásconez-Maza, M.D., Charroud, M., 2023. Integration of electrical resistivity tomography and seismic refraction tomography to investigate subsiding Sinkholes in Karst areas. Water 15 (12), 2192. https://doi.org/10.3390/w15122192.

Karaman, A., Karadayılar, T., 2004. Identification of karst features using seismic P-wave tomography and resistivity anisotropy measurements. Environ. Geol. 45, 957–962. https://doi.org/10.1007/s00254-003-0953-4.

Kaufmann, O., Deceuster, J., Quinif, Y., 2012. An electrical resistivity imaging-based strategy to enable site-scale planning over covered palaeokarst features in the Tournaisis area (Belgium). Eng. Geol. 133, 49–65. https://doi.org/10.1016/j.enggeo.2012.01.017.

Kim, J.W., Lu, Z., Kaufmann, J., 2019. Evolution of sinkholes over Wink, Texas, observed by high-resolution optical and SAR imagery. Remote Sens. Environ. 222, 119–132. https://doi.org/10.1016/j.rse.2018.12.028.

Kuniansky, E.L., Weary, D.J., Kaufmann, J.E., 2016. The current status of mapping karst areas and availability of public sinkhole-risk resources in karst terrains of the United States. Hydrogeol. J. 24 (3), 613. https://doi.org/10.1007/s10040-015-1333-3.

Liu, R., Sun, H., Qin, J., Zheng, Z., 2023. A multi-geophysical approach to assess potential sinkholes in an urban area. Eng. Geol. 318, 107100 https://doi.org/10.1016/j.enggeo.2023.107100.

Loke, M.H., Acworth, I., Dahlin, T., 2003. A comparison of smooth and blocky inversion methods in 2D electrical imaging surveys. Explor. Geophys. 34 (3), 182–187. https://doi.org/10.1071/EG03182.

Loke, M.H., Chambers, J.E., Rucker, D.F., Kuras, O., Wilkinson, P.B., 2013. Recent developments in the direct-current geoelectrical imaging method. J. Appl. Geophys. 95, 135–156. https://doi.org/10.1016/j.jappgeo.2013.02.017.

Martinez-Moreno, F.J., Galindo-Zaldivar, J., Pedrera, A., Teixido, T., Ruano, P., Peña, J. A., González-Castillo, L., Ruiz-Constán, A., López-Chicano, M., Martin-Rosales, W., 2014. Integrated geophysical methods for studying the karst system of Gruta de las Maravillas (Aracena, Southwest Spain). J. Appl. Geophys. 107, 149–162. https://doi.org/10.1016/j.jappgeo.2014.05.021.

Martinez-Moreno, F.J., Galindo-Zaldivar, J., Pedrera, A., González-Castillo, L., Ruano, P., Calaforra, J.M., Guirado, E., 2015. Detecting gypsum caves with microgravity and ERT under soil water content variations (Sorbas, SE Spain). Eng. Geol. 193, 38–48. https://doi.org/10.1016/j.enggeo.2015.04.011.

Martinez-Pagan, P., Gómez-Ortiz, D., Martin-Crespo, T., Manteca, J.I., Rosique, M., 2013. The electrical resistivity tomography method in the detection of shallow mining cavities. A case study on the Victoria Cave, Cartagena (SE Spain). Eng. Geol. 156, 1–10. https://doi.org/10.1016/j.enggeo.2013.01.013.

Martinez-Segura, M.A., Garcia-Nieto, M.C., Navarro, M., Vásconez-Maza, M.D., Oda, Y., Garcia-Jerez, A., Enomoto, T., 2024. Seismic characterisation of the subsoil under a historic building: Cathedral Church of Saint Mary in Murcia case study. Eng. Geol. 335, 107529 https://doi.org/10.1016/j.enggeo.2024.107529.

Nasseri-Moghaddam, A., Cascante, G., Phillips, C., Hutchinson, D.J., 2007. Effects of underground cavities on Rayleigh waves—Field and numerical experiments. Soil Dyn. Earthq. Eng. 27 (4), 300–313. https://doi.org/10.1016/j.soildyn.2006.09.002.

Papadopoulos, N.G., Tsourlos, P., Tsokas, G.N., Sarris, A., 2007. Efficient ERT measuring and inversion strategies for 3D imaging of buried antiquities. Near Surf. Geophys. 5 (6), 349–361. https://doi.org/10.3997/1873-0604.2007017.

Porsani, J.L., Walter Filho, M., Elis, V.R., Shimeles, F., Dourado, J.C., Moura, H.P., 2004. The use of GPR and VES in delineating a contamination plume in a landfill site: a case study in SE Brazil. J. Appl. Geophys. 55 (3–4), 199–209. https://doi.org/10.1016/j.jappgeo.2003.11.001.

Rahnema, H., Mirassi, S., Dal Moro, G., 2021. Cavity effect on Rayleigh wave dispersion and P-wave refraction. Earthq. Eng. Eng. Vib. 20, 79–88. https://doi.org/10.1007/s11803-021-2006-y.

Reynolds, J.M., 2011. An Introduction to Applied and Environmental Geophysics. John Wiley & Sons.

Robert, T., Dassargues, A., Brouyère, S., Kaufmann, O., Hallet, V., Nguyen, F., 2011. Assessing the contribution of electrical resistivity tomography (ERT) and self-potential (SP) methods for a water well drilling program in fractured/karstified limestones. J. Appl. Geophys. 75 (1), 42–53. https://doi.org/10.1016/j.jappgeo.2011.06.008.

Saribudak, M., 2011. Urban geophysics: geophysical signature of the Mount Bonnell Fault and its Karstic Features in Austin, Texas. Houston Geol. Soc. Bull. 54 (2), 49–54.

Saribudak, M., 2016. Geophysical mapping of Mount Bonnell fault of Balcones fault zone and its implications on Trinity-Edwards Aquifer interconnection, Central Texas, USA. Lead. Edge 35 (9), 752–758. https://doi.org/10.1190/tle35090752.1.

Saribudak, M., Hauwert, N.M., 2017. Integrated geophysical investigations of Main Barton Springs, Austin, Texas, USA. J. Appl. Geophys. 138, 114–126. https://doi.org/10.1016/j.jappgeo.2017.01.004.

Sevil, J., Gutiérrez, F., Zarroca, M., Desir, G., Carbonel, D., Guerrero, J., Linares, R., Roqué, C., Fabregat, I., 2017. Sinkhole investigation in an urban area by trenching in combination with GPR, ERT and high-precision leveling. Mantled evaporite karst of Zaragoza city, NE Spain. Eng. Geol. 231, 9–20. https://doi.org/10.1016/j.enggeo.2017.10.009.

Sharp Jr., J.M., Green, R.T., Schindel, G.M., 2019. The Edwards Aquifer: The Past, Present, and Future of a Vital Water Resource. Geological Society of America, Memoir 215, Boulder, Colorado, USA.

Sheehan, J.R., Doll, W.E., Watson, D.B., Mandel, W., 2005. Detecting cavities with seismic refraction tomography: Can it be done?. In: 18th EEGS Symposium on the Application of Geophysics to Engineering and Environmental Problems, 989–1003. European Association of Geoscientists & Engineers, Environ. and Eng. Geophys. Soc, Atlanta, GA. https://doi.org/10.3997/2214-4609-pdb.183.989-1003.

Shevnin, V., Mousatov, A., Ryjov, A., Delgado-Rodriquez, O., 2007. Estimation of clay content in soil based on resistivity modelling and laboratory measurements. Geophys. Prospect. 55 (2), 265–275. https://doi.org/10.1111/j.1365-2478.2007.00599.x.

Sloan, S.D., Nolan, J.J., Broadfoot, S.W., McKenna, J.R., Metheny, O.M., 2013. Using near-surface seismic refraction tomography and multichannel analysis of surface waves to detect shallow tunnels: a feasibility study. J. Appl. Geophys. 99, 60–65. https://doi.org/10.1016/j.jappgeo.2013.10.004.

Sloan, S.D., Schwenk, J.T., Stevens, R.H., Butler, B.W., 2015. Hazard assessment and site characterization at an oil and gas well site using surface wave methods. In: International Conference on Engineering Geophysics, Al Ain, United Arab Emirates. Society of Exploration Geophysicists, pp. 114–117. https://doi.org/10.1190/iceg2015-032.

Wang, D., Lv, L.J., 2023. Analysis of Rayleigh wave response characteristics in complicated cave system and detection methods. Mech. Syst. Signal Process. 185, 109806 https://doi.org/10.1016/j.ymssp.2022.109806.

Xie, J., Huang, J., Lu, J., Burton, G.J., Zeng, C., Wang, Y., 2022. Development of two-dimensional ground models by combining geotechnical and geophysical data. Eng. Geol. 300, 106579 https://doi.org/10.1016/j.enggeo.2022.106579.

Xu, C., Butt, S.D., 2006. Evaluation of MASW techniques to image steeply dipping cavities in laterally inhomogeneous terrain. J. Appl. Geophys. 59 (2), 106–116. https://doi.org/10.1016/j.jappgeo.2005.08.003.

Yi, M.J., Kim, J.H., Song, Y., Cho, S.J., Chung, S.H., Suh, J.H., 2001. Three-dimensional imaging of subsurface structures using resistivity data. Geophys. Prospect. 49 (4), 483–497. https://doi.org/10.1046/j.1365-2478.2001.00269.x.